A Novel Cross-Domain Data Augmentation and Bearing Fault Diagnosis Method Based on an Enhanced Generative Model

Shilong Sun, *Member, IEEE*, Hao Ding, Haodong Huang, Zida Zhao, Dong Wang, *Member, IEEE*, and Wenfu Xu, *Senior Member, IEEE*

***Abstract*— In actual industrial production, differences in product ion conditions lead to variations in the collected data distribution. This gives rise to a particular problem: while one set of conditions has complete status data available, another set only possesses data from the healthy state. Differences in data conditions result in limitations for diagnosing the new condition. To address this challenge, a method based on envelope order spectra for data generation is proposed. Initially, envelope and order analysis are conducted on raw vibration data to align envelope spectra across different domains and extract domain-independent signal components—the envelope order spectra. Subsequently, an enhanced variational autoencoder generative adversarial network (VAEGAN) is trained using the envelope order spectra. The trained model is then employed to generate synthetic envelope order spectra, serving as data augmentation for another set of working conditions, thereby achieving cross-domain data augmentation. Next, the augmented envelope order spectra data are used to train a generic model for fault classification, enabling cross-domain fault diagnosis. Finally, the proposed approach is validated by testing it with real envelope order spectra data from a different working condition. Experimental results demonstrate that the proposed method can generate reliable fake data under diverse working conditions, accomplishing cross-domain data augmentation and fault diagnosis while preserving data privacy.**

***Index Terms*— Cross-domain data augmentation, data imbalance, envelope order spectrum (EOS), fault diagnosis, variational autoencoder generative adversarial networks (VAEGANs).**

Manuscript received 12 January 2024; revised 14 March 2024; accepted 3 April 2024. Date of publication 17 April 2024; date of current version 1 May 2024. This work was supported in part by the Program of Shenzhen Peacock Innovation Team, Guangdong, China under Grant KQTD20210811090146075; in part by the Basic Research Program of Shenzhen under Grant JCYJ20220818102415034; in part by the Guangdong Basic and Applied Basic Research Foundation under Grant 2021A1515110615 and Grant 2024A1515012041; and in part by the Shenzhen Higher Education Stability Support Plan under Grant GXWD20231130195340002. The Associate Editor coordinating the review process was Dr. Ke Feng. *(Corresponding author: Shilong Sun.)*

Shilong Sun, Hao Ding, Haodong Huang, and Zida Zhao are with the School of Mechanical Engineering and Automation and Guangdong Provincial Key Laboratory of Intelligent Morphing Mechanisms and Adaptive Robotics, Harbin Institute of Technology, Shenzhen 518055, China (e-mail: sunshilong@hit.edu.cn; dinghao_ouc@126.com; hhd1340201839@163.com; a1320943099@163.com).

Dong Wang is with the State Key Laboratory of Mechanical System and Vibration, Shanghai Jiao Tong University, Shanghai 200240, China (e-mail: dongwang4-c@sjtu.edu.cn).

Wenfu Xu is with the Guangdong Provincial Key Laboratory of Intelligent Morphing Mechanisms and Adaptive Robots, Key University Laboratory of Mechanism and Machine Theory and Intelligent Unmanned Systems of Guangdong, Harbin Institute of Technology, Shenzhen 518052, China (e-mail: wfxu@hit.edu.cn).

Digital Object Identifier 10.1109/TIM.2024.3390242

I. Introduction

In THE realm of modern manufacturing, real-time monitoring has become a ubiquitous practice for overseeing equipment within factories. This proactive approach empowers engineers to continually evaluate the health status of equipment based on monitored data, facilitating the timely identification and precise diagnosis of potential faults. Building on this foundation, engineers and factory managers can swiftly collaborate to address faults, implement intelligent scheduling schemes, and effectively manage and rectify issues. This comprehensive strategy aims to proactively mitigate safety and economic risks associated with equipment failures. Notably, among the crucial components of rotating machinery products, rolling bearings assume a pivotal role. Operating under demanding conditions, including high-speed operations and heavy loads, these bearings often endure prolonged periods of continuous operation in actual production processes. Consequently, they represent a primary focus for health monitoring initiatives. If the bearing fails, it can affect the overall performance of the mechanical equipment, causing downtime, expensive maintenance, and hidden costs to the enterprise. In severe cases, it can even lead to serious safety accidents.

Recently, many scholars have committed themselves to developing effective and accurate fault diagnosis methods for rolling bearings, aiming to ensure their seamless operation and enhance the safety and economic benefits of mechanical products. These methods can be categorized into traditional signal processing-based diagnostic approaches and data-driven intelligent diagnostic methods, catering to the requirements of subjective analysis and reasoning. Traditional fault diagnosis methods, which are based on signal processing, aim to detect and diagnose faults in complex, dynamic signals (e.g., vibrations) with low signal-to-noise ratios. These methods use techniques, such as denoising, filtering, time–frequency analysis, and signal decomposition, to extract fault features [1]. They have been applied in the health management of critical equipment, such as offshore wind turbines [2], intelligent manufacturing systems [3], and key components, such as bearings and gears. Specifically, signal processing techniques, such as wavelet transform [4], wavelet packet transform [5], Hilbert–Huang transform (HHT) [6], and empirical mode decomposition (EMD) [7], are classic and commonly used technical tools in this context. In recent years, they have seen

wide application and rapid development in the signal analysis of mechanical fault diagnosis. However, this process is complex and less intelligent than current data-driven methods.

With the advent of the era of big industrial data, intelligent diagnostic methods have attracted significant attention due to their robustness and ability to make complex calculations, such as convolutional neural networks (CNNs) [8], autoencoder (AE) [9], and deep belief networks (DBNs) [10], among others. Liu et al. [11] proposed a fault detection method utilizing acoustic emission signals, combining wavelet region correlation threshold denoising (WRCTD) and a fusion of operational modal analysis (OMA) and variational mode decomposition (VMD) for enhanced efficacy. Peng et al. [12] proposed a residual neural network for intelligent fault diagnosis with bearing-free-label contrastive learning (BYOL). Xu et al. [13] proposed a cross-modal fusion CNN (CMFCNN) for mechanical fault diagnosis to address the issue of data distribution gap from multisource mechanical signals. Wang et al. [14] introduced a fully interpretable neural network that utilizes statistical quantities to replace extreme learning machines (ELMs) for machine state detection. Sun et al. [15] proposed a CNN collaborative fault diagnosis method under the framework of swarm learning to address the issue of insufficient data. Meanwhile, Sun et al. [16] also proposed a method that utilizes wavelets and filters as a substitute for CNN, aiming to capture distinctions among various local models. Hou et al. [17] proposed a data-driven optimized square envelope spectrum, termed OSESgram, for selecting the optimal informative frequency bands (IFBs) in vibration-based bearing fault diagnosis. In addition, Zhou et al. [18] established a new semisupervised method for dealing with limited training data based on deep convolutional generative adversarial networks (DCGANs). Xiao et al. [19] proposed a joint transfer network for unsupervised bearing fault diagnosis, transferring from simulation domain to experimental domain. Zuo et al. [20] introduced a probabilistic spike response model (PSRM) with a multilayer structure to improve the performance of SNN in bearing fault diagnosis. Su et al. [21] proposed a data reconstruction hierarchical recursive meta-learning (DRHRML) method for bearing fault diagnosis under different working conditions. Finally, Yan et al. [22] proposed a novel weight-oriented optimization model for simultaneous interpretable initial fault detection and fault diagnosis. In essence, artificial intelligence (AI) has propelled the advancement of real-time data-driven intelligent fault diagnosis, showcased remarkable potential, and attracted increased attention. Nevertheless, these sophisticated fault diagnosis methods often require substantial datasets, and practical industrial applications frequently face challenges related to inconsistent data distribution, commonly known as domain shift. This issue substantially impairs the performance of data-driven models.

Within the domain of data-driven fault diagnosis, the ceiling is often determined by the quality and quantity of data, a common challenge encountered in practical production. In real-world applications, available training data are rarely perfect and frequently lack either in quantity or quality. For instance, within the fault history dataset of a particular factory, there is an abundance of data samples for common and frequently occurring fault types, but a shortage of samples for rare faults. In the event of a rare fault occurring in a critical component, a model trained on such a dataset may struggle to provide timely and reliable diagnoses, potentially leading to severe consequences. Moreover, the vibration data distribution of the same bearing can vary under different operating conditions. If the training data do not fully align with the operational scenarios, the model's generalization capability may be compromised. As a result, it is essential to explore the insufficient availability of labeled training data and the challenges of training across various working conditions.

Data generative models [23] are a viable approach to deal with data insufficiency. These models generate similar sample data by learning the characteristics of the original existing sample data, forming enough data to work with. A generative adversarial network (GAN) [24] is a representative data generation model, which solves the problem of insufficient samples by expanding sample data. It has been widely used in the field of image analysis and is now also applied in bearing fault diagnosis. Therefore, in the scenario of insufficient training data, leveraging the existing data to train a generative model and subsequently utilizing the newly generated data for data augmentation emerge as a viable solution. Nevertheless, in actual production scenarios, varied working conditions might yield adequate fault data collection in one scenario, posing challenges or encountering sample shortages in another. This situation may result in the generative model, trained on the existing data, producing generated data that do not completely align with the authentic distribution, particularly lacking in generated data for specific conditions. Many fault diagnosis studies overlook practical application scenarios, prioritizing idealized laboratory simulations. Thus, we aim to minimize the impact of cross-condition variations during the data generation phase by considering real-world production scenarios.

In response to the scarcity of labeled fault data for certain bearings in practical production and the challenges posed by domain differences between training and testing data leading to poor generalization, this article proposes an effective method for generating fault data. Specifically, Hilbert transformation and fast Fourier transformation (FFT) are applied to the time-domain signals from sensors. Subsequently, an order analysis is conducted on the resulting envelope spectrum to extract signal components unrelated to the domain, obtaining an envelope order spectrum (EOS). Next, an EOS-based variational autoencoder GAN (EOS-VAEGAN) is designed to form a generative model. Leveraging the EOS data, this model generates fault data adaptable to different working conditions. The main contributions of this article are as follows.

1) This article employs an enhanced VAEGAN to generate data samples for data augmentation, effectively addressing the problem of insufficient labeled data under specific working conditions prior to model training.
2) The proposed method extracts the EOS of the fault signal, isolating fault characteristics with weak associations to working conditions as the training set for the generative model. This approach effectively addresses the domain shift issue between training and testing data, enabling the generated data to efficiently meet

the requirements for training diagnostic models under various working conditions.

3) The generated pseudo-data not only compensate for the shortage of training data but also ensure data privacy protection. Moreover, by combining the generated synthetic fault data with the original normal data, the model remains capable of training an effective fault diagnostic model.

The remainder of this article is organized as follows. Section II provides a brief overview of envelope extraction, order analysis, and the related research on VAEGAN. Section III describes the detailed process of the proposed method, including the structure of the diagnostic model and the data preprocessing steps for converting the data into an EOS. Section IV presents the experimental results of using the proposed method on bearing fault signals and comparative experiments. Section V concludes this article.

II. Related Fundamental Work

A. Envelope Extraction

The envelope spectrum is a frequency-domain signal analysis method that adeptly demodulates and extracts bearing impact signals embedded in high-frequency natural vibrations. Consequently, it enables the effective detection of fault features in the frequency domain.

The process of envelope extraction involves several steps. First, the Hilbert transform is applied to the input signal, generating an analytical signal. Then, the modulus of the analytical signal is calculated, yielding the envelope signal. This envelope signal can be further analyzed by performing FFT, which yields the Hilbert envelope spectrum. The resulting spectrum shows the amplitude of the envelope signal as a function of frequency. The envelope spectrum is a powerful tool for detecting vibration and shock in a signal.

If the input signal is denoted by $x(t)$, then its Hilbert transform $\hat{x}(t)$ can be computed as follows:

$$\hat{x}(t) = \frac{1}{\pi}\int_{-\infty}^{+\infty}\frac{x(t-\tau)}{\tau}d\tau = x(t)\cdot\frac{1}{\pi}. \tag{1}$$

In (1), the output of the signal after passing through a series of orthogonal filters is represented. To further process this signal, an analytic signal can be constructed, which is a complex signal derived from the original real signal. The purpose of constructing the analytic signal is to obtain a representation of the signal in the complex domain. To achieve this, the analytic signal can be expressed as a combination of the original signal and its Hilbert transform, which is obtained by shifting the phase of the Fourier transform of the signal by $-\pi/2$. Mathematically, the analytic signal can be expressed as follows:

$$\tilde{x}(t) = x(t) + j\hat{x}(t) = A(t)e^{j\varphi(t)} \tag{2}$$

where $x(t)$ is the real part of the signal, $\hat{x}(t)$ is its imaginary part, and j is the imaginary unit. $A(t)$ of the signal is the Hilbert envelope of $x(t)$. The envelope spectrum is obtained by doing Fourier transform on this $A(t)$.

Diverging from conventional spectra, the amplitude of the fault characteristic frequency stands out conspicuously in the envelope spectrogram, facilitating more straightforward identification. Consequently, envelope spectrum analysis proves to be more apt for extracting fault characteristics when compared with traditional spectrum analysis.

B. Order Analysis

Order analysis [25] is a crucial method for dealing with rotational speed and order. The order, which is primarily relevant to rotating machinery, represents the number of times a rotating part completes a full rotation in a specific time frame. The order is a multiple of the rotational speed or rotational frequency and remains constant for the rotational speed. The actual speed, which is independent of the axis, is a multiple or fraction of the speed of the reference axis. In general, the vibration and noise response of the structure appear at multiples or fractions of the rotational speed, known as orders.

In real industrial production equipment, the rotational speed of the machinery fluctuates to some extent rather than remaining constant. This fluctuation causes a change in the rotation frequency, and consequently, the fault characteristic frequency of the bearing also changes. At this point, a conventional Fourier spectrum analysis in steady-state conditions is ineffective. To overcome the limitations of conventional FFT and other methods in fault diagnosis of variable speed rotating machinery, scholars have developed the order analysis method, also referred to as the order-tracking method.

The key to order-tracking technology is to sample the constant angle of the reference axis and perform Fourier transform on the angle-domain stationary waveform to obtain the frequency spectrum. This spectrum reflects the amplitude and frequency distribution of different orders of vibration in the bearing. Since rolling bearings operate at different speeds and loads under different working conditions, the spectrum under various working conditions cannot correspond. However, the corresponding relationship between order spectra is relatively accurate. By resampling the sampling signals at equal time intervals, the software transforms them into equiangular spaced sampling signals, enabling one-to-one correspondence of spectral lines under different working conditions.

The relationship among order, frequency, and speed can be expressed as follows:

$$O = 60f/n \tag{3}$$

where O is the order of the measured object, which is a unitless quantity; f is the frequency of the measured object in hertz (Hz); and n is the speed of the motor in revolutions per minute (RPM).

C. Generative Model

As a pivotal category within AI models, generative models receive training samples adhering to the distribution p_{raw}. They acquire the ability to emulate this data distribution and generate a probabilistic model, denoted as p_{model}, allowing for

the production of data samples resembling the training set for subsequent utilization. Notably, GANs and VAEs stand out as the two primary generative models in this context.

GAN [26] is comprised of a pair of neural networks, a discriminator (D) and a generator (G), which are based on statistics and game theory to generate data samples. The primary goal of GAN is to input random noise (z) into G to generate data, with the data generated by G being referred to as pseudo-samples. Subsequently, the fake and real samples are inputted to D simultaneously to distinguish between them. The purpose of D is to identify fake samples from real samples accurately, while G aims to generate data similar to the original data. Therefore, D and G compete against each other to achieve their goals. The ultimate objective of the GAN model is to make the accuracy rate of G distinguish between fake and real samples 0.5, which ensures that the fake samples appear genuine.

GAN aims to let the generator generate enough samples to fool the discriminator. From a statistical point of view, assume that the generated pseudo-samples and real samples have the same data distribution; that is, the generated samples and real samples have the same probability density function, that is, $p_G(x) = p_{\text{data}}(x)$. The purpose of training GAN is also to meet this requirement. The loss function of GAN comes from the cross-entropy loss function of the two classifications

$$L = -\frac{1}{N_i}\left[y_i \log p_i + (1 - y_i)\log(1 - p_i)\right]. \tag{4}$$

The loss function of the discriminator is divided into two parts; one part is to discriminate the real sample as 1, and the other part is to discriminate the fake sample as 0, so the optimization goal of the discriminator is to maximize the sum of these two items; using $V(\text{G}, \text{D})$, the optimization objective is

$$V(\text{G}, \text{D}) = \text{E}_{x\sim p_{\text{data}}(x)} \log(\text{D}(x)) + \text{E}_{z\sim p_z(z)} \log(1 - \text{D}(x)) \tag{5}$$

$$\text{D}_{\text{G}}^{*} = \arg\max_{\text{D}} V(\text{G}, \text{D}). \tag{6}$$

The purpose of the generator is to compete with the discriminator and aims at making (5) as small as possible. The generator G^{*} can be expressed as follows:

$$\text{G}^{*} = \arg\min_{\text{G}} V\left(\text{G}, \text{D}_{\text{G}}^{*}\right). \tag{7}$$

Regarding VAE, it innovates upon the foundation of AEs by incorporating variational inference theory. This involves constraining the distribution q of learned latent variables z to approximate a predefined prior distribution p, typically a standard normal distribution. Thus, beyond the conventional reconstruction loss $L(x, \hat{x})$, VAE introduces the Kullback–Leibler (K–L) divergence loss to ensure a more uniform distribution of latent variables in the latent space

$$L = L(x, \hat{x}) + \sum_{j} \text{KL}(q_j(z|x)||p(z)). \tag{8}$$

VAE achieves enhanced robustness of the decoder to noise by introducing Gaussian noise to the results of the encoder. Simultaneously, it employs K–L loss for regularization of the encoder, aiming to drive the mean of the encoded distribution toward zero. In addition, the encoder outputs variance to modulate the intensity of the noise, imparting a certain level of randomness and variability to the decoder's output. This approach facilitates the learning of more generalized results.

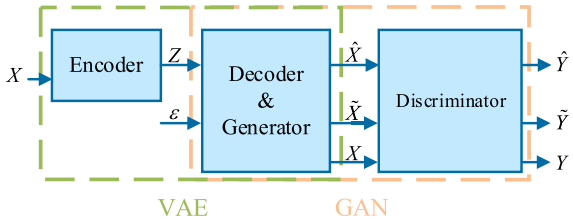

Fig. 1. Structure of VAEGAN.

Hence, through adversarial learning, GANs iteratively strengthen sample generation, achieving higher quality outputs. Nevertheless, their training may be vulnerable to challenges, such as mode collapse and instability. In contrast, VAEs, by constraining latent variables within a prior distribution, imbue the latent space with enhanced continuity, thereby facilitating interpolation within latent representations.

Fig. 1 shows the VAEGAN model, which integrates VAE onto the foundation of GAN to enhance training stability. The two models share a common decoder, amalgamating the continuity from VAE and the generative capabilities of GAN in the latent space. This integration allows for semantic-meaningful interpolation within the latent space. Achieving a fine equilibrium between VAE and GAN, the model excels in producing samples that exhibit superior qualities in terms of quality, diversity, and control over the latent space.

III. Procedure of the Proposed Method

This section illustrates the proposed envelope-order-spectrum-based method for VAEGAN data generation (EOS-VAEGAN).

A. Overall Process

This section provides an overview of the proposed method, which involves utilizing the EOS signals as the input of VAEGAN to generate samples. Assume that there are multiple sets of data in different working conditions. One set of data have all faulty data, but the other set of data have only normal data. The data from the first working condition undergo analysis and processing to obtain the EOS. This EOS is then used as the input for the VAEGAN network, which generates the pseudo-EOS. Use the generated pseudo-EOS and the EOS of the normal data under the second working condition to train a network and finally use the data of the second working condition to input the final network to test the feasibility of the network. The flowchart of the whole algorithm is shown in Fig. 2.

B. Envelope Order Spectrum

For the original data, initial preprocessing is conducted. Subsequently, Hilbert transformation based on (1) and (2) is applied, followed by FFT transformation, to obtain the signal's envelope spectrum. Subsequently, the frequency of the envelope spectrum signal is linearly interpolated and divided by the

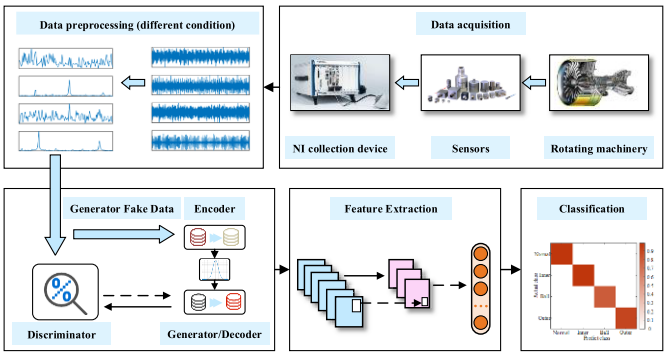

Fig. 2. Flowchart of the proposed algorithm.

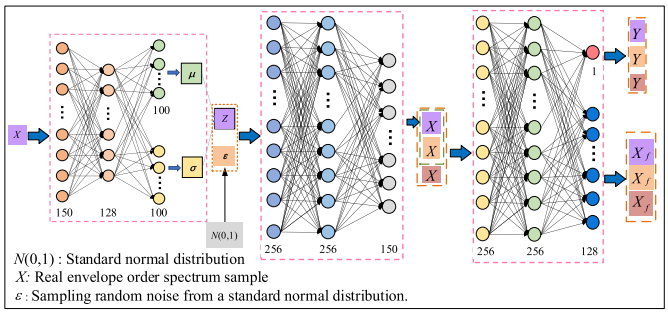

Fig. 3. Structure of the enhanced VAEGAN model.

rotational speed [see (3)] to obtain the order, resulting in the EOS, which will serve as the real input for subsequent model generation. In this process, the envelope spectrum processing transforms the signal from the time domain to the frequency domain, effectively demodulating the signal and extracting the fault characteristics, making the fault information more significant and less likely to be lost. Furthermore, when conducting order analysis on the envelope spectrum signal, due to the minimal impact of load variation on the signal, we focus primarily on the differences in speed between signals from different working conditions. Under varying speeds, the fault characteristic frequency of the collected signals is positively correlated with the speed. We perform order analysis based on (3), which essentially conducts analysis processing in the angular domain, to reduce the differences caused by speed variations, aligning the envelope spectra from different speeds. Therefore, after extracting the EOS from signals under different working conditions, not only have we achieved some degree of fault feature extraction, but we have also reduced the differences caused by speed changes, to some extent extracting domain-independent fault feature components.

C. Enhanced VAEGAN

The enhanced VAEGAN model structure, as illustrated in Fig. 3, is composed of three components: an encoder, a decoder (which also serves as a generator), and a discriminator. During the forward propagation process, the envelop order spectrum data X of the original input are processed by the encoder to obtain μ and σ. Subsequently, the encoding result Z is computed based on the following equation:

$$Z = \mu + e^{\sigma/2} \cdot \varepsilon'. \tag{9}$$

Following this, a portion of random noise data ε is sampled from a standard normal distribution. This noise data, along with Z, are separately fed into the decoder, resulting in the generated envelop order spectrum $\widetilde{X}$ and the reconstructed envelop order spectrum $\widehat{X}$. Furthermore, $\widehat{X}$, $\widetilde{X}$, and X are individually input into the discriminator, yielding discrimination results ($\widehat{Y}$, $\widetilde{Y}$, Y) and feature extraction results ($\widehat{X}_f$, $\widetilde{X}_f$, X_f).

While training the model, an adversarial approach is still indispensable. Consequently, for each epoch, it is imperative to initially fix the parameters of both the encoder and decoder and then proceed to update the parameters of the discriminator. During the training of the discriminator, the loss function is defined, as illustrated in the following equation:

$$L_{\text{dis}} = L_{\text{CE}}(Y, \mathbf{1}) + L_{\text{CE}}(\widetilde{Y}, \mathbf{0}) + \alpha \cdot L_{\text{CE}}(\widehat{Y}, \mathbf{0}) \tag{10}$$

where L_{CE} denotes the cross-entropy loss, and $\mathbf{0}$ and $\mathbf{1}$ represent the all-zero and all-one vectors, respectively.

Following the parameter update of the discriminator, its parameters are fixed for the subsequent training of the encoder and decoder, i.e., the VAE portion. The training loss function for this section is depicted in (15), comprising three main components. Equation (11) represents the generative adversarial loss, employing the discriminator to adversarial train the generation of data to closely resemble ground truth. Equation (12) signifies the generative matching loss, ensuring alignment between generated data and ground-truth data through the discriminator's outcomes. Equation (14) corresponds to the K–L divergence loss, aiming to bring the distribution of encoded data as close as possible to a normal distribution

$$L_{\text{GD}} = L_{\text{CE}}(\widetilde{Y}, \mathbf{1}) \tag{11}$$

$$L_{\text{Grec}} = \frac{\beta}{N}\left(\gamma \cdot \text{MSE}(X, \widehat{X}) + \text{MSE}(X_f, \widehat{X}_f)\right) \tag{12}$$

$$\text{MSE}(X, Y) = \frac{1}{m \cdot n}\sum_{i=1}^{m}\sum_{j=1}^{n}\left(X_{ij} - Y_{ij}\right)^2 \tag{13}$$

$$L_{\text{KL}} = -\frac{1}{2}\sum_{i=1}^{N}\left(1 + \boldsymbol{\sigma}_i - \boldsymbol{\mu}_i^2 - e^{\boldsymbol{\sigma}_i}\right) \tag{14}$$

$$L_{\text{VAE}} = \omega_1 \cdot L_{\text{KL}} + \omega_2 \cdot L_{\text{GD}} + \omega_3 \cdot L_{\text{Grec}}. \tag{15}$$

In this context, an additional feature extraction component has been incorporated into the design of the last layer of the discriminator, aiming to perform more than just data classification. The purpose of this operation is to compute the squared difference between the generated EOS data in the discriminator's feature space and the real EOS data. Consequently, the generator's matching loss encompasses both the matching loss based on the discriminator's classification results and the discriminator's feature matching loss. By minimizing this loss, our objective is for the feature distribution of the generated data in the discriminator's feature space to closely resemble the feature distribution of real data. This contributes to the generator producing more authentic EOS data.

Ultimately, the loss function for the VAE component is the weighted sum of three individual losses. In (10)–(15), parameters ω_1, ω_2, and ω_3 serve as hyperparameters, allowing

TABLE I
CNN PARAMETERS SETUP

Layer	Tied parameter	Activation function	Output size
Input	/	/	16×150×1
Convolutional layer 1	Kernel size: 16, Filters: 32 Stride:2	ReLU	16×68×32
Pooling layer 1	Pool_size: 2 Stride:2	/	16×34×32
Convolutional layer 2	Kernel size: 8, Filters: 64 Stride:1	ReLU	16×27×64
Pooling layer 2	Pool_size: 2 Stride: 2	/	16×13×64
Convolutional layer 3	Kernel size: 4, Filters: 128 Stride:1	ReLU	16×5×128
Pooling layer 3	Pool_size: 3 Stride: 3	/	16×1×128
Flatten	/	/	16×128
Dense 1	Units: 180	ReLU	16×180
Dense 2	Units: 4	Softmax	16×4

for flexible adjustment of the weights assigned to different loss components.

D. CNNs Parameters Setup

After obtaining the generated data, the dataset with missing values is enhanced. To assess the effectiveness of the augmented dataset, a basic CNN model can be employed as a classification model. The model is trained using the generated data, while the original authentic data serve as the test set to evaluate the quality of generating data across different operating conditions. The network structure parameters of the CNN model are presented in Table I.

E. Algorithmic Pseudocode

A pseudocode for the proposed cross-domain fault diagnosis algorithm has been developed. First, the data from each operating condition are collected. Subsequently, in the scenario where fault data are abundant for one operating condition (source domain) and scarce for another (target domain), cross-domain data augmentation and fault diagnosis are conducted. Specifically, the data from the source domain are preprocessed to obtain the EOS of the fault signals for that operating condition. Following this, an enhanced VAEGAN model is trained using these EOS data as a training set. The trained model is then utilized to generate synthetic data for the source domain. Subsequently, the generated synthetic data, along with the limited real data from the target domain, are combined to form a training set for a fault classification model of the target domain.

Our experiment purpose is to effectively validate the outcomes of cross-domain data augmentation and fault diagnosis. Deliberately, abundant data in both the source and target domains were opted for. However, it is essential to note that the fault data from the target domain are exclusively reserved for use as a test set. This strategic choice is made to assess the effectiveness of cross-domain fault diagnosis. Consequently, the target domain is still considered to lack sufficient training data for fault scenarios.

Algorithm 1 Cross-Domain Fault Diagnosis Algorithm

I. Obtain data for each working condition

II. Data preprocessing

Perform the envelope order for the data (N_1, N_2, ..., I_1, I_2, ..., B_1, B_2, ..., O_1, O_2, ...,) of each working condition (C = 1,2,3,...),

Perform linear interpolation on the obtained data of various operating conditions, and set the length to 150.

III. Data generation

Select data from one domain as the source domain and data from another domain as the target domain,

Source domain data $S_{I,B,O}$ (data of three fault types) and random noise input GAN are trained.

For any epoch, j = 1, 2, 3, ..., n,

$$L_{dis} = L_{CE}(Y, \mathbf{1}) + L_{CE}(\widetilde{Y}, \mathbf{0}) + \alpha \cdot L_{CE}(\widehat{Y}, \mathbf{0})$$
$$L_{VAE} = \omega_1 \cdot L_{KL} + \omega_2 \cdot L_{GD} + \omega_3 \cdot L_{Grec}$$

IV. Fault classification

Input random noise into VAEGAN to generate 3 types of faults, with a data volume of 3 × 460 × 150,

Aggregate the normal data of the target domain and the generated data to form a complete data 4 × 460 × 150,

Use this complete data (N_{real2}, I_{fake1}, B_{fake1}, O_{fake1}) as the training data for training the CNN model;

Take the data T (N_{real2}, I_{real2}, B_{real2}, O_{real2}) of the target domain as the test set.

TABLE II
DATASET'S WORKING CONDITIONS

Bearing Health Status	Motor Load (HP)	Approx. Motor Speed (rpm)	Fault Diameter
Normal	0	1797	\
	1	1772	\
	2	1750	\
	3	1730	\
Inner Race	0	1797	0.007"
	1	1772	0.007"
	3	1750	0.007"
	4	1730	0.007"
Ball	0	1797	0.007"
	1	1772	0.007"
	2	1750	0.007"
	3	1730	0.007"
Outer Race	0	1797	0.007"
	1	1772	0.007"
	2	1750	0.007"
	3	1730	0.007"

IV. EXPERIMENTAL RESULTS AND COMPARISONS

A. Dataset Preparation

This section provides an overview of the data preprocessing steps employed for input into the neural network. In our experimental setup, the publicly available dataset from Case Western Reserve University (CWRU) was utilized. To obtain the subsamples for our VAEGAN input, preprocessing of the dataset was undertaken. The sampling frequency is 12k, and the fault data in the file are 10-s long. The list of subdatasets used is provided in Table II.

TABLE III
EXPERIMENTAL DATA DIVISION

Experiment Number	Training set (working conditions)	Test set (working conditions)
E I	1	2
E II	1	3
E III	1	4
E IV	2	3
E V	2	4
E VI	3	4

TABLE IV
EXPERIMENTAL PARAMETER DESIGN

Parameter	Value	Parameter	Value
VAEGAN Epoch	41	VAEGAN Learning Rate	0.0001
VAEGAN Batch Size	16	Noise Length	100
Latent dimension	100	α	0.5
β	0.5	γ	0.01
ω_1	1	ω_2	1
ω_3	0.01	CNN Learning Rate	0.0001
CNN Epoch	20	CNN Batch Size	16

The first step involves partitioning the entire dataset into multiple subsamples, and each subsignal is defined with a length of 10 000 data points. Within the dataset files, a substantial volume of data pertains to the normal state of the bearing. The data step size for normal bearings is set at 500, whereas for faulty bearings, it is 240. This results in a total of 620 groups of normal data and 460 groups of fault data.

1) Envelope spectrum and order analysis are performed on each set of data with a length of 10 000, resulting in an EOS with a length of 5000.
2) By calculating the fault frequency of the bearing and converting it into the fault order, it is determined that the fault order of the inner ring fault, outer ring fault, and rolling element is between 2.5 and 8.
3) The EOS with a data length of 5000 is interpolated to the fault order range using linear interpolation, resulting in a final data length of 150.

B. Experimental Dataset Group Division

During the experiment, the data from working condition 1 were divided into three parts: inner ring fault, rolling element fault, and outer ring fault. These three sets of data were used as real sample inputs for VAEGAN to generate corresponding synthetic fault data. For working condition 2, only normal data were used for training, obtained after preprocessing the data. The data length for the three types of faults in working condition 1 was $3 \times 460 \times 150$, while the length of normal data for working condition 2 was 620×150, and the fault data length was $3 \times 460 \times 150$. Among these, 460 groups of normal data were used for training and 160 groups for testing. The experiment was conducted with four health states of the bearing, including normal, inner ring failure, rolling element failure, and outer ring failure. The data, initially assigned numbers 0, 1, 2, and 3 according to the load, represented four unique working conditions, each characterized by different speed and load parameters. These subsets were subsequently renumbered 1, 2, 3, and 4 based on the associated load, with each new number denoting a specific combination of speed and load. This resulted in a total of six groups, as shown in Table III.

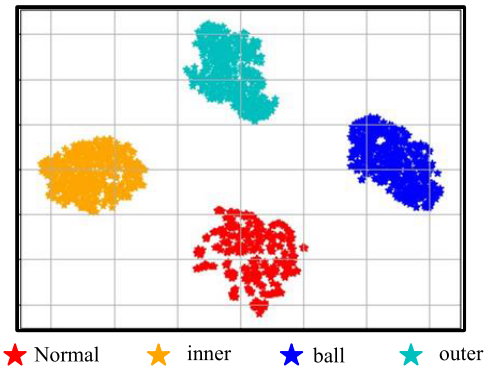

Fig. 4. t-SNE feature dimensionality reduction plot of generated data.

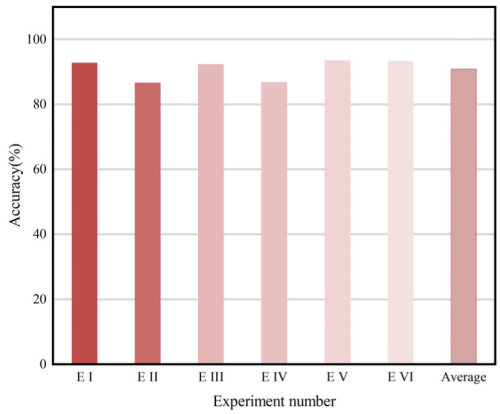

Fig. 5. Six sets of experimental results of four different working conditions.

C. Experimental Results and Discussion

In this experiment, the learning rate, training batch, and other experimental parameters involved are shown in Table IV.

During the experiment, the data t-SNE feature dimensionality reduction map after VAEGAN was generated, as shown in Fig. 4. It is clearly classified into four groups because of four kinds of fault.

Consistent results across multiple experiments were noted, and the result of one of these experiments was selected for presentation, as illustrated in Fig. 5, with the respective accuracies of 92.81%, 86.72%, 92.34%, 86.88%, 93.44%, and 93.28%. The data in the experiment were in four working conditions and six migrations, respectively. From Fig. 5, during the migration process, the average accuracy was basically over 90%, which indicates that the proposed method is indeed effective.

In order to reflect the superiority of the proposed method, we proceeded to compare the approach outlined in this article with the FFT spectrum-based method. In order to reflect the single variable of the experiment, the dimensionality of the data was maintained throughout the preprocessing steps. Following the FFT transformation, the fault characteristic frequency was determined and confirmed. In this context, data within the frequency range of 20–200 Hz were selected and interpolated linearly to yield a dataset of 150 points.

As depicted in Fig. 6, it is evident that, when considering FFT-VAEGAN as the control experiment, its multiple

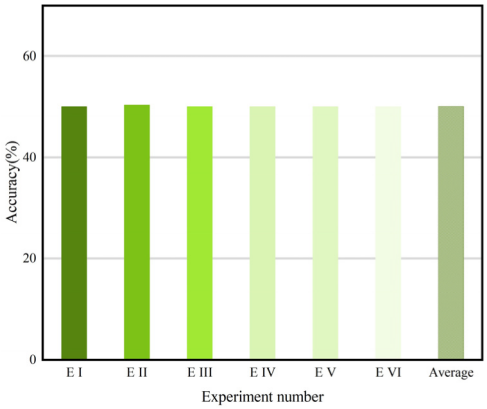

Fig. 6. Results of the baseline.

TABLE V
MULTIPLE SETS' RESULTS OF EXPERIMENTAL COMPARISONS

Accuracy / Model	E I (%)	E II (%)	E III (%)	E IV (%)	E V (%)	E VI (%)	Mean (%)
FFT_GAN	50.0	50.0	50.0	57.7	36.7	48.9	49.1
FFT-WGAN	74.7	75.0	51.9	75.0	51.9	51.9	63.4
FFT_VAE	75.8	75.0	75.3	74.8	58.3	69.2	71.4
FFT_VAEGAN	50.0	50.3	50.0	50.0	50.0	50.0	50.1
EOS-GAN	86.1	89.7	95.5	85.3	83.6	76.1	86.1
EOS-WGAN	50.3	70.3	80.2	70.3	80.2	80.2	71.9
EOS-VAE	83.0	91.4	94.6	77.7	84.7	84.1	85.9
EOS-VAEGAN	92.8	86.7	92.3	86.9	93.4	93.3	90.9

TABLE VI
COMPARISON OF EOS-VAEGAN, MAML, DAN, AND SNN

	Accuracy (%)	Time (s)
EOS-VAEGAN	94.83±1.21	274.11
MAML[27]	90.89±1.70	1063.21
DAN[28]	90.36±4.58	1333.64
SNN[29]	91.76±5.34	198.76

sets of experimental results hover around 50%, significantly inferior to the performance of EOS-VAEGAN. This outcome further corroborates the effectiveness of the EOS in extracting domain-independent fault characteristics and, consequently, the efficacy of our proposed methodology.

Then, we maintained the structure of the fault diagnosis model and varied the data generation approach, conducting multiple sets of experimental comparisons, as illustrated in Table V.

Through comparison with experiments using other methods, it is evident that the EOS can effectively reduce the domain difference between different working conditions and narrow the data distribution of the two domains. In contrast, the Fourier spectrum is significantly influenced by the equipment's working conditions.

To further validate the effectiveness and reliability of the model, additional reproducibility experiments were conducted. The mean and variance of multiple experiment results were computed, and comparisons were made with several algorithms for small-sample fault diagnosis, including model-agnostic meta-learning (MAML), domain adaptation network (DAN), and Siamese neural network (SNN) algorithms. The comparative results are presented in Table VI. The results from the table clearly demonstrate that our proposed EOS-VAEGAN method outperforms in terms of both average performance and reliability.

V. CONCLUSION

This article proposes an enhanced VAEGAN data generation method based on the EOS that spans the data from one working condition to another, ensuring data privacy while providing diagnostic guidelines for healthy conditions. The method effectively addresses the challenge of insufficient labeled training data under new working conditions, achieving cross-domain data augmentation and fault diagnosis, all while safeguarding data privacy. Currently, using the data to create the EOS involves extracting characteristics that are independent of work condition. These characteristics are then used to provide pseudo-features to equipment under other working conditions, which can be tested using its own unique characteristics. Through comparative experiments, the average accuracy of the six migration experiments reached 94.83%. The feasibility of this method has been verified, fully utilizing the information in the data.

Despite achieving satisfactory results, the current application focus is on bearings; thus, we have gained an understanding of the failure frequency of bearings. Subsequently, further research will be conducted to apply this technology to other industrial equipment and components, such as pumps, reducers, and gearbox.

REFERENCES

[1] Y. Li, Y. Yang, K. Feng, M. J. Zuo, and Z. Chen, "Automated and adaptive ridge extraction for rotating machinery fault detection," *IEEE/ASME Trans. Mechatronics*, vol. 28, no. 5, pp. 2565–2575, Apr. 2023.

[2] K. Feng, J. C. Ji, K. Wang, D. Wei, C. Zhou, and Q. Ni, "A novel order spectrum-based vold-Kalman filter bandwidth selection scheme for fault diagnosis of gearbox in offshore wind turbines," *Ocean Eng.*, vol. 266, Dec. 2022, Art. no. 112920.

[3] K. Feng, J. C. Ji, Q. Ni, Y. Li, W. Mao, and L. Liu, "A novel vibration-based prognostic scheme for gear health management in surface wear progression of the intelligent manufacturing system," *Wear*, vol. 522, Jun. 2023, Art. no. 204697.

[4] W. Hu, J. Yuan, H. Jiang, Q. Zhao, C. Li, and Z. Yao, "Tensor denoising assisted time-reassigned synchrosqueezing wavelet transform for gear fault diagnosis," *IEEE Trans. Instrum. Meas.*, vol. 72, pp. 1–12, 2023.

[5] L. Wang, Z. Liu, H. Cao, and X. Zhang, "Subband averaging Kurtogram with dual-tree complex wavelet packet transform for rotating machinery fault diagnosis," *Mech. Syst. Signal Process.*, vol. 142, Aug. 2020, Art. no. 106755.

[6] Z. Liu, D. Peng, M. J. Zuo, J. Xia, and Y. Qin, "Improved Hilbert–Huang transform with soft sifting stopping criterion and its application to fault diagnosis of wheelset bearings," *ISA Trans.*, vol. 125, pp. 426–444, Jun. 2022.

[7] S. Gao, Q. Wang, and Y. Zhang, "Rolling bearing fault diagnosis based on CEEMDAN and refined composite multiscale fuzzy entropy," *IEEE Trans. Instrum. Meas.*, vol. 70, pp. 1–8, 2021.

[8] Y. Xue, R. Yang, X. Chen, Z. Tian, and Z. Wang, "A novel local binary temporal convolutional neural network for bearing fault diagnosis," *IEEE Trans. Instrum. Meas.*, vol. 72, pp. 1–13, 2023.

[9] M. Shi et al., "Deep hypergraph autoencoder embedding: An efficient intelligent approach for rotating machinery fault diagnosis," *Knowl.-Based Syst.*, vol. 260, Jan. 2023, Art. no. 110172.

[10] Y. Liu, X. Wang, Z. Zeng, W. Zhang, and H. Qu, "An event-driven spike-DBN model for fault diagnosis using reward-STDP," *ISA Trans.*, vol. 140, pp. 55–70, Sep. 2023.

[11] L. Liu, Z. Zhi, Y. Yang, S. Shirmohammadi, and D. Liu, "Harmonic reducer fault detection with acoustic emission," *IEEE Trans. Instrum. Meas.*, vol. 72, pp. 1–12, 2023.

[12] T. Peng, C. Shen, S. Sun, and D. Wang, "Fault feature extractor based on bootstrap your own latent and data augmentation algorithm for unlabeled vibration signals," *IEEE Trans. Ind. Electron.*, vol. 69, no. 9, pp. 9547–9555, Sep. 2022.
[13] Y. Xu et al., "Cross-modal fusion convolutional neural networks with online soft-label training strategy for mechanical fault diagnosis," *IEEE Trans. Ind. Informat.*, vol. 20, no. 1, pp. 73–84, Jan. 2024.
[14] D. Wang, Y. Chen, C. Shen, J. Zhong, Z. Peng, and C. Li, "Fully interpretable neural network for locating resonance frequency bands for machine condition monitoring," *Mech. Syst. Signal Process.*, vol. 168, Apr. 2022, Art. no. 108673.
[15] S. Sun, H. Huang, T. Peng, C. Shen, and D. Wang, "A data privacy protection diagnosis framework for multiple machines vibration signals based on a swarm learning algorithm," *IEEE Trans. Instrum. Meas.*, vol. 72, pp. 1–9, 2023.
[16] S. Sun, H. Huang, T. Peng, and D. Wang, "An improved data privacy diagnostic framework for multiple machinery components data based on swarm learning algorithm," *IEEE Trans. Instrum. Meas.*, vol. 72, pp. 1–9, 2023.
[17] B. Hou, Y. Chen, H. Wang, Z. Peng, K. Tsui, and D. Wang, "OSESgram: Data-aided method for selection of informative frequency bands for bearing fault diagnosis," *IEEE Trans. Instrum. Meas.*, vol. 71, pp. 1–10, 2022.
[18] K. Zhou, E. Diehl, and J. Tang, "Deep convolutional generative adversarial network with semi-supervised learning enabled physics elucidation for extended gear fault diagnosis under data limitations," *Mech. Syst. Signal Process.*, vol. 185, Feb. 2023, Art. no. 109772.
[19] Y. Xiao, H. Shao, S. Han, Z. Huo, and J. Wan, "Novel joint transfer network for unsupervised bearing fault diagnosis from simulation domain to experimental domain," *IEEE/ASME Trans. Mechatronics*, vol. 27, no. 6, pp. 5254–5263, Dec. 2022.
[20] L. Zuo, F. Xu, C. Zhang, T. Xiahou, and Y. Liu, "A multi-layer spiking neural network-based approach to bearing fault diagnosis," *Rel. Eng. Syst. Saf.*, vol. 225, Sep. 2022, Art. no. 108561.
[21] H. Su, L. Xiang, A. Hu, Y. Xu, and X. Yang, "A novel method based on meta-learning for bearing fault diagnosis with small sample learning under different working conditions," *Mech. Syst. Signal Process.*, vol. 169, Apr. 2022, Art. no. 108765.
[22] T. Yan, D. Wang, and Y. Wang, "Discrimination- and sparsity-driven weight-oriented optimization model for interpretable initial fault detection and fault diagnosis," *IEEE Trans. Instrum. Meas.*, vol. 73, pp. 1–13, 2024.
[23] K. Rombach, G. Michau, and O. Fink, "Controlled generation of unseen faults for partial and open-partial domain adaptation," *Rel. Eng. Syst. Saf.*, vol. 230, Feb. 2023, Art. no. 108857.
[24] R. Wang, Z. Chen, and W. Li, "Gradient flow-based meta generative adversarial network for data augmentation in fault diagnosis," *Appl. Soft Comput.*, vol. 142, Jul. 2023, Art. no. 110313.
[25] T. Li, Z. Peng, H. Xu, and Q. He, "Parameterized domain mapping for order tracking of rotating machinery," *IEEE Trans. Ind. Electron.*, vol. 70, no. 7, pp. 7406–7416, Jul. 2023.
[26] Y. Li, F. Xu, and C.-G. Lee, "Self-supervised metalearning generative adversarial network for few-shot fault diagnosis of hoisting system with limited data," *IEEE Trans. Ind. Informat.*, vol. 19, no. 3, pp. 2474–2484, Mar. 2023.
[27] S. Zhang, F. Ye, B. Wang, and T. G. Habetler, "Few-shot bearing fault diagnosis based on model-agnostic meta-learning," *IEEE Trans. Ind. Appl.*, vol. 57, no. 5, pp. 4754–4764, Sep. 2021.
[28] J. Zhu, N. Chen, and C. Shen, "A new multiple source domain adaptation fault diagnosis method between different rotating machines," *IEEE Trans. Ind. Informat.*, vol. 17, no. 7, pp. 4788–4797, Jul. 2021.
[29] J. Zhao et al., "A novel hierarchical training architecture for Siamese neural network based fault diagnosis method under small sample," *Measurement*, vol. 215, Jun. 2023, Art. no. 112851.

Shilong Sun (Member, IEEE) received the Ph.D. degree from the City University of Hong Kong, Hong Kong, in 2018.

He is currently an Assistant Professor with Harbin Institute of Technology, Shenzhen, China. He nurtures keen interests in vibration energy harvesting design, fault diagnosis and prognosis, decision-making with artificial intelligence (AI), and deep learning for industrial data. Now, he focuses on the remaining equipment life estimation research with deep learning and smart energy harvesting techniques.

Hao Ding was born in Bozhou, China. He received the B.S. degree in marine engineering from the School of Engineering, Ocean University of China, Qingdao, China, in 2022. He is currently pursuing the M.S. degree in mechanical engineering with the School of Mechanical Engineering and Automation, Harbin Institute of Technology, Shenzhen, China.

His research interests include intelligent fault diagnosis and graph learning.

Haodong Huang was born in Jingmen, China. He received the B.S. degree in mechanical engineering from the School of Mechanical Engineering and Automation, University of Northeast of China, Shenyang, China, in 2021. He is currently pursuing the M.S. degree in mechanical engineering with the School of Mechanical Engineering and Automation, Harbin Institute of Technology, Shenzhen, China.

His research interests include mechanical fault diagnosis and condition monitoring.

Zida Zhao was born in Xingtai, China. He received the B.S. degree in mechanical engineering from the North China Electric Power University, Beijing, China, in 2022. He is currently pursuing the M.S. degree in mechanical engineering with the School of Mechanical Engineering and Automation, Harbin Institute of Technology, Shenzhen, China.

His research interests include mechanical fault diagnosis and biped robot.

Dong Wang (Member, IEEE) received the Ph.D. degree from the City University of Hong Kong, Hong Kong, in 2015.

He was a Senior Research Assistant, a Post-Doctoral Fellow, and a Research Fellow with the City University of Hong Kong. He is currently an Associate Professor with the Department of Industrial Engineering and Management, Shanghai Jiao Tong University, Shanghai, China, where he is also with the State Key Laboratory of Mechanical System and Vibration. His research interests include sparse and complex measures, signal processing, prognostics and health management, condition monitoring and fault diagnosis, statistical learning and machine learning, statistical process control, and nondestructive testing.

Dr. Wang is an Editorial Board Member of Mechanical Systems and Signal Processing. He is an Associate Editor of IEEE TRANSACTIONS ON INSTRUMENTATION AND MEASUREMENT, *Measurement*, IEEE SENSORS JOURNAL, and *Journal of Dynamics Monitoring and Diagnostics*.

Wenfu Xu (Senior Member, IEEE) received the B.E. and M.E. degrees in control engineering from Hefei University of Technology, Hefei, China, in 2001 and 2003, respectively, and the Ph.D. degree in control science and engineering from Harbin Institute of Technology, Harbin, China, in 2007.

He was a Research Associate with the Department of Mechanical and Automation Engineering, The Chinese University of Hong Kong, Hong Kong. He is currently a Professor with the School of Mechanical Engineering and Automation, Harbin Institute of Technology, Shenzhen, China. His research interests include reconfigurable robots, space robots, and bionic robots.